SUPPORTING INFORMATION

Lead Free Hybrid Halide Perovskite based Piezo/Triboelectric Self-Powered Wearable Dual-functional Sensors

Abinash Tiwari[a], Niloy Mridha[b], Sumit Kumar Sharma[a], Monika Salesh[b], Chandra Mouli Nannapaneni [b], Prasanna Kumar Mural[b], Aswani Yella*[a,b]

a – Centre for Research in Nanotechnology and Science, Indian Institute of Technology, Bombay, 400076.

b – Department of Metallurgical Engineering and Material Science, Indian Institute of Technology, Bombay, 400076.

Corresponding Author e-mail: aswani.yella@iitb.ac.in

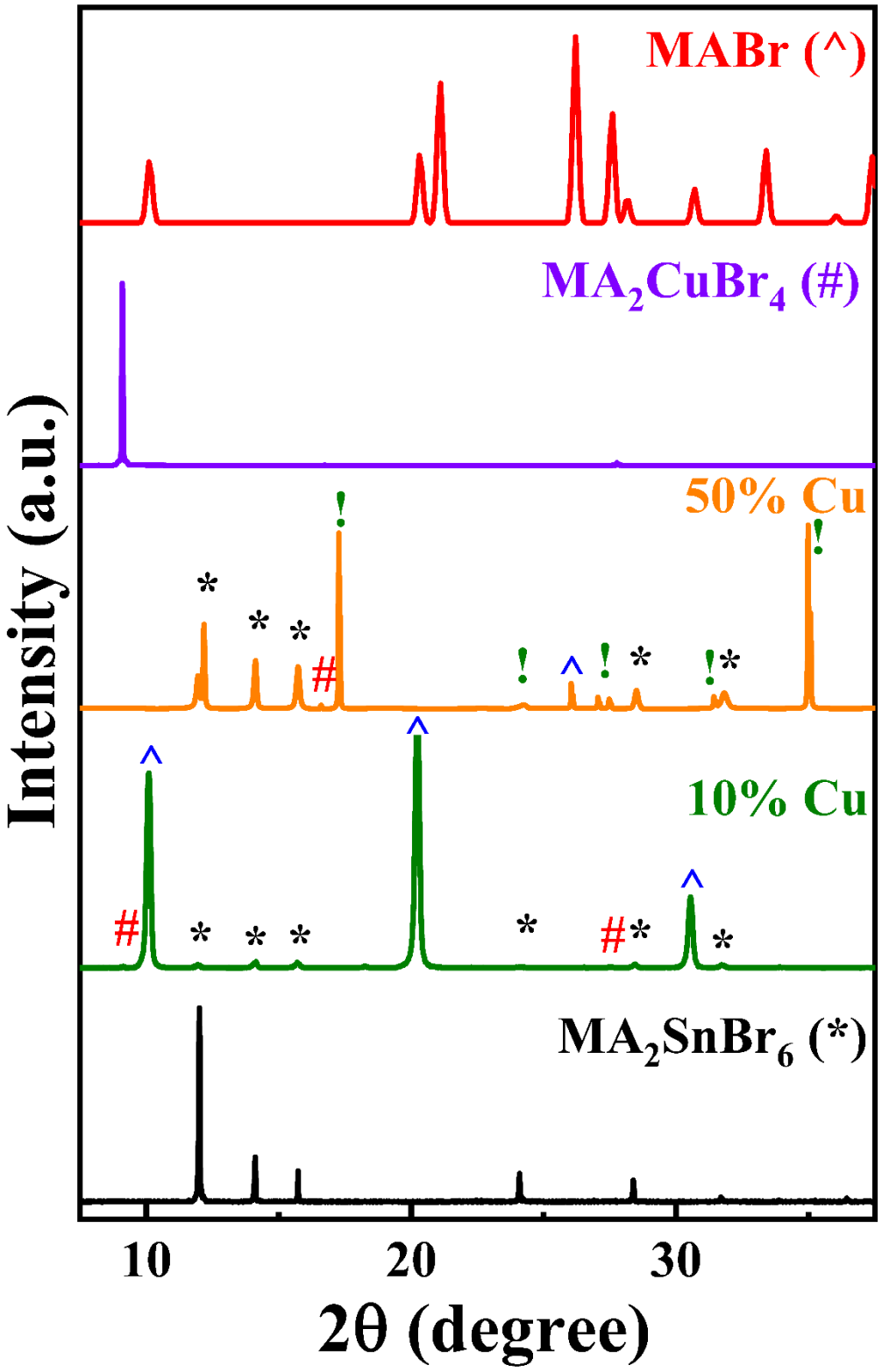

Figure S1. XRD spectra of 10% Cu and 50% Cu films compared with MA_2SnBr_6, MABr and MA_2CuBr_4.

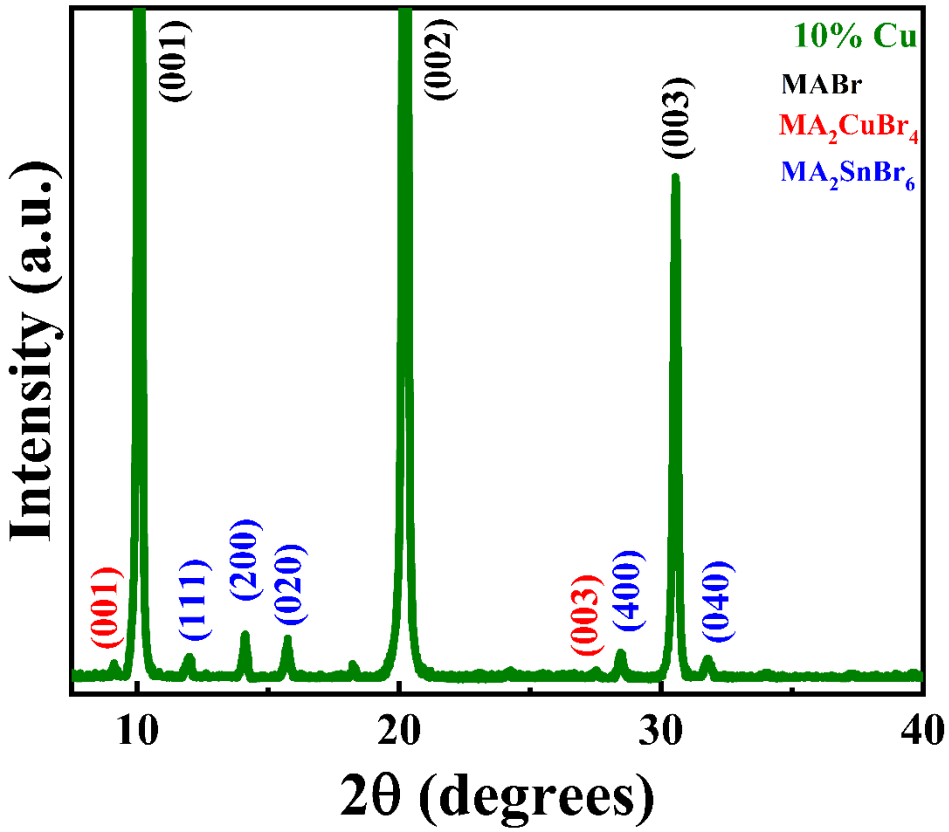

Figure S2. XRD of the 10% Cu material.

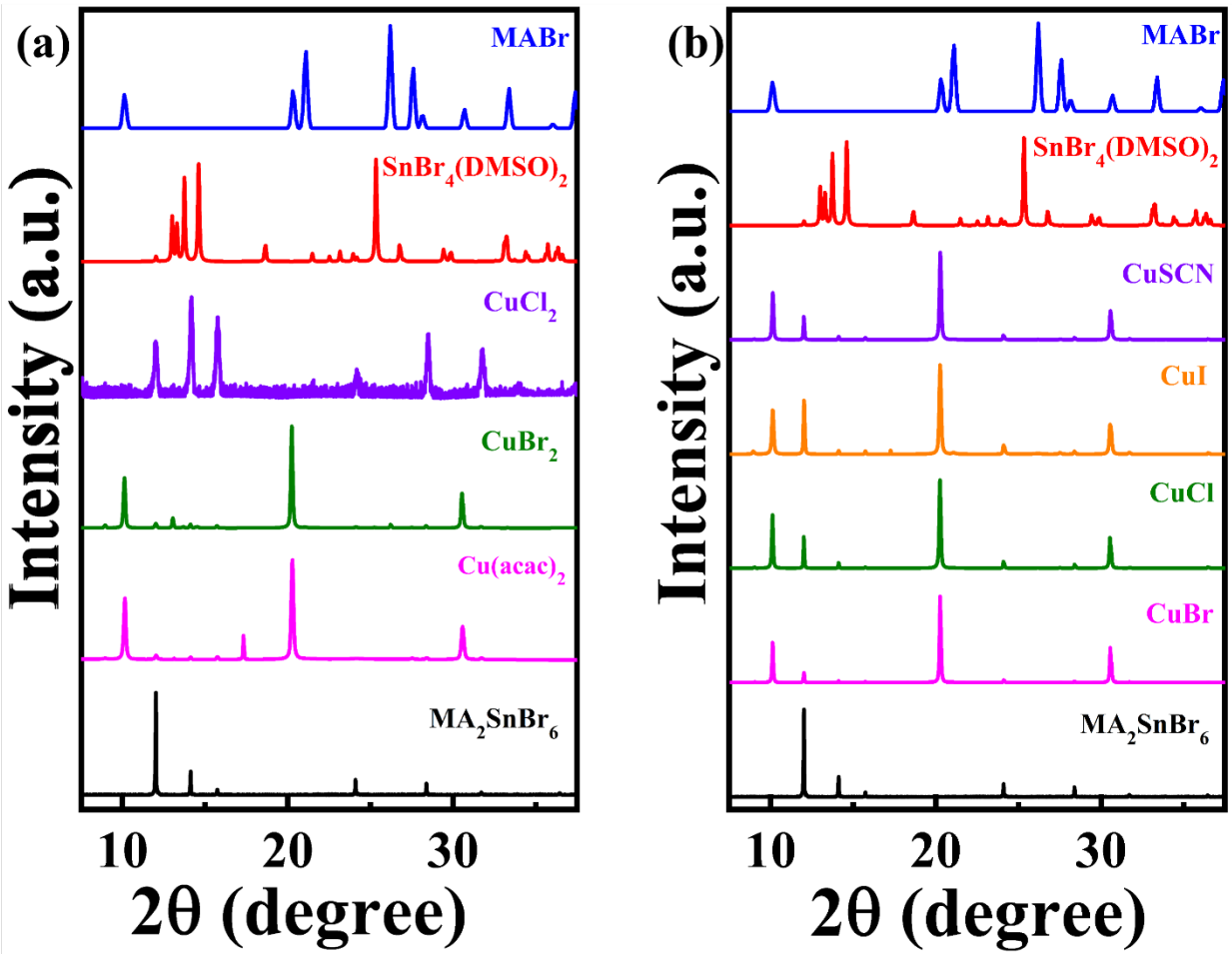

Figure S3. XRD of 0.1 CuX prepared using different (a) Cu (II) salts and, (b) Cu (I) salts.

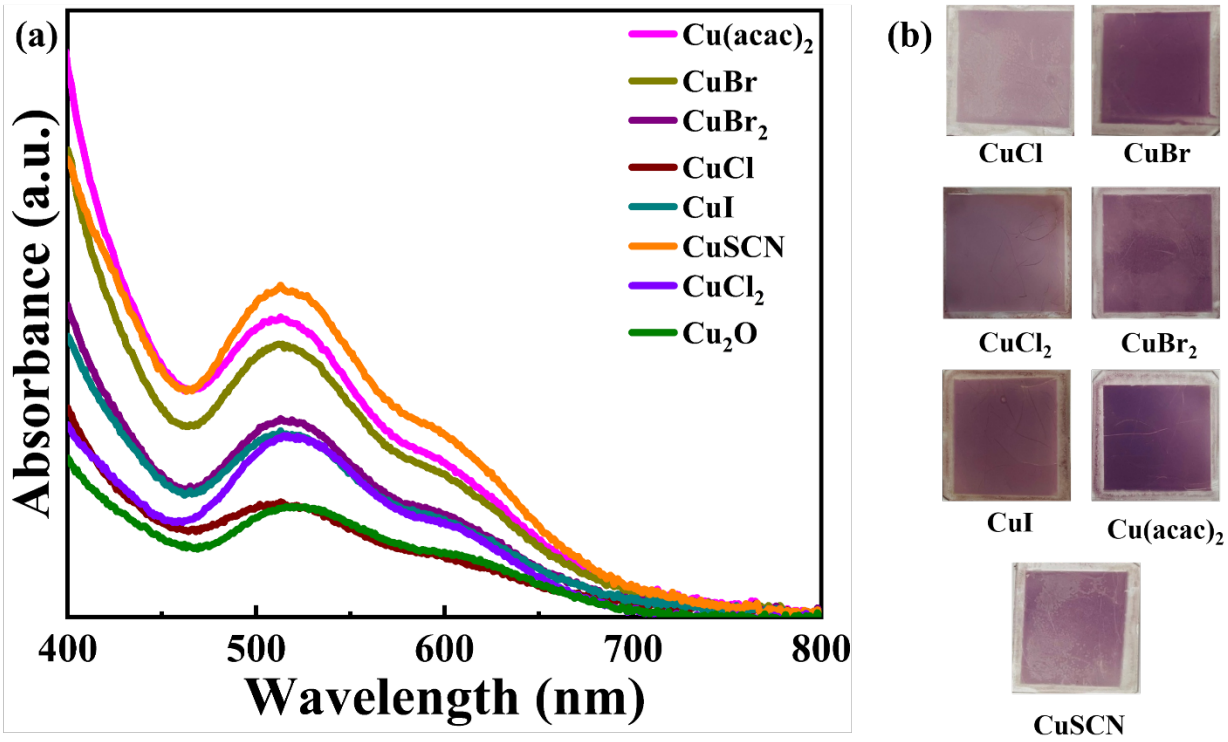

Figure S4. (a) UV-Visible absorbance spectra and, (b) Images of 0.1 CuX material prepared using different Cu (I and II) salts.

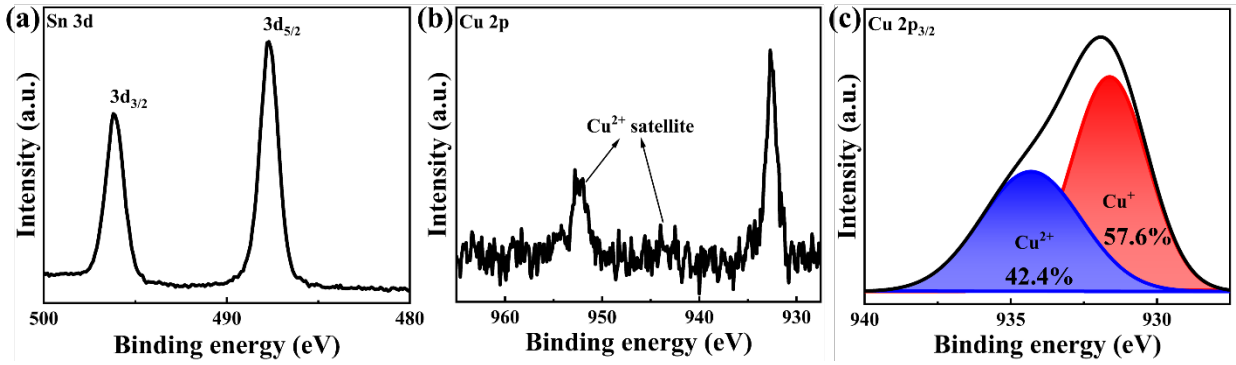

Figure S5. XPS spectrum of (a) tin and, (b) copper in 10% Cu material. (c) Percentage distribution of Cu^{+} and Cu^{2+} in the Cu $2p_{3/2}$ peak.

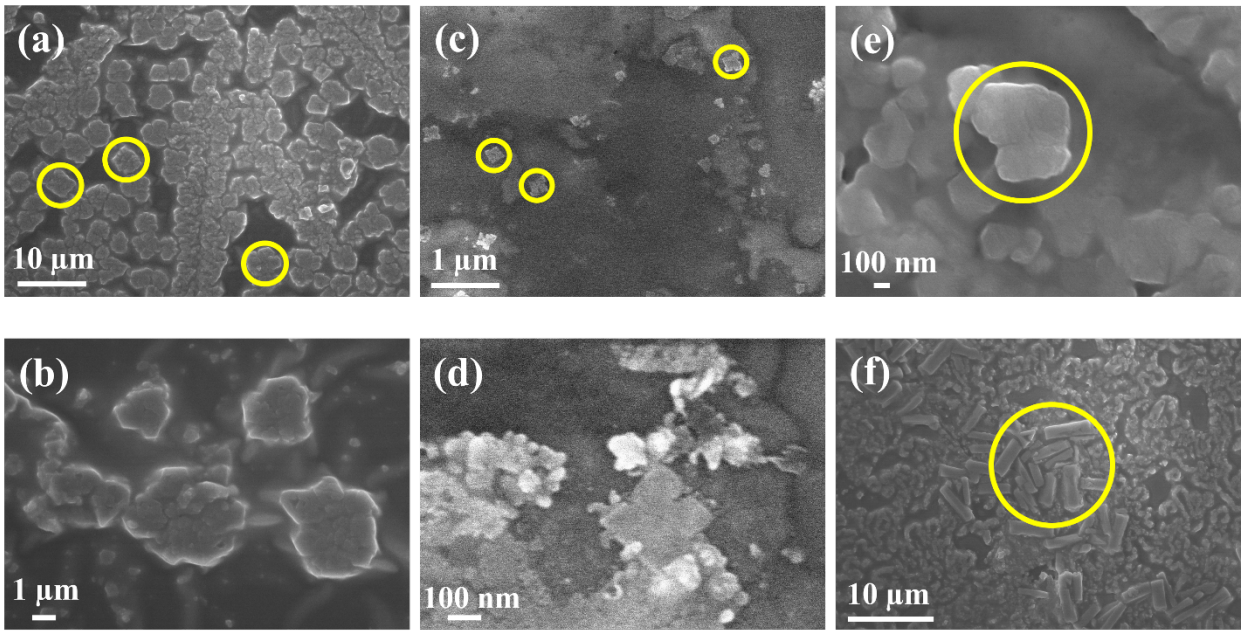

Figure S6. (a), (b) are that of MA_2SnBr_6 (Irregular chunks, particle size: ~5 µm); (c), (d) are that of MA_2CuBr_4 (Cubes, particle size: ~200 nm), and (e), (f) are that of 10% $CuCl_2$ in MABr:$SnBr_2$ (4:1) in DMSO.

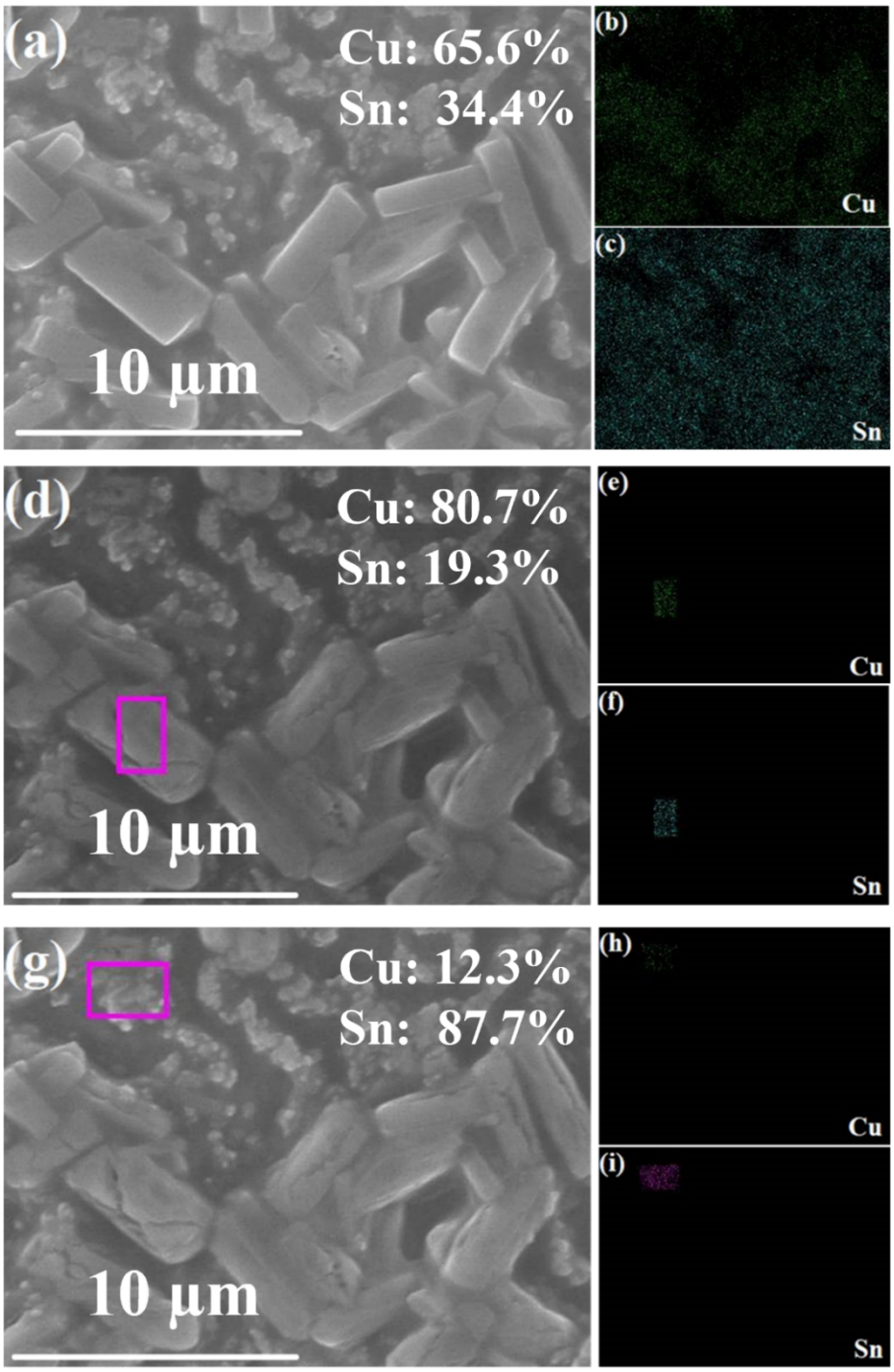

Figure S7. EDS analysis of the 10% $CuCl_2$ in MABr:$SnBr_2$ (4:1) in DMSO, (a) corresponds to the mapping over the entire area ((b) and (c) are the Cu and Sn distribution) , (d) mapping over the cuboid particles ((e) and (f) are the Cu and Sn distribution), and (g) mapping of the irregular chunks ((h) and (i) are the Cu and Sn distribution). The MA_2CuBr_4 based crystals grow in size while the MA_2SnBr_6 crystal size decreases.

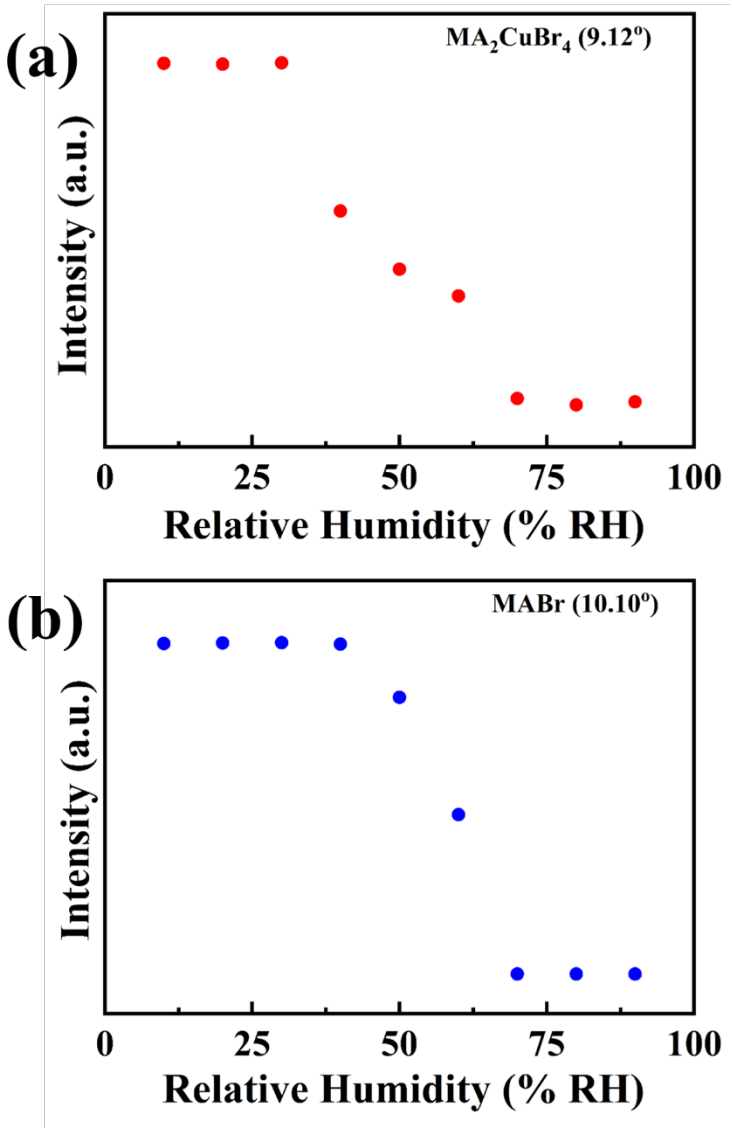

Figure S8. In-situ XRD, (a) MA_2CuBr_4 (9.12°) and (b) MABr (10.10°) peak at different RH%.

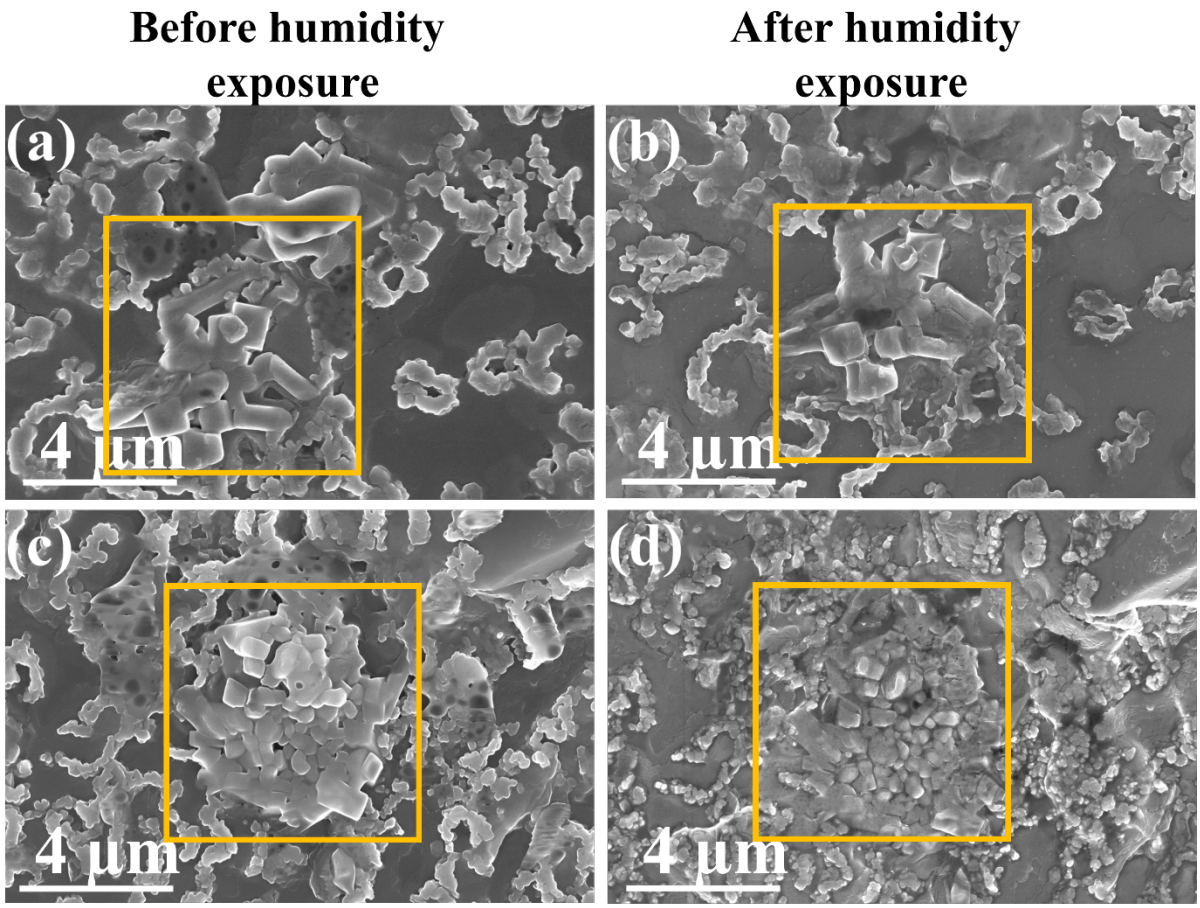

Figure S9: (a), (c) 10% Cu film before humidity exposure. (b), (d) 10% Cu film after humidity exposure.

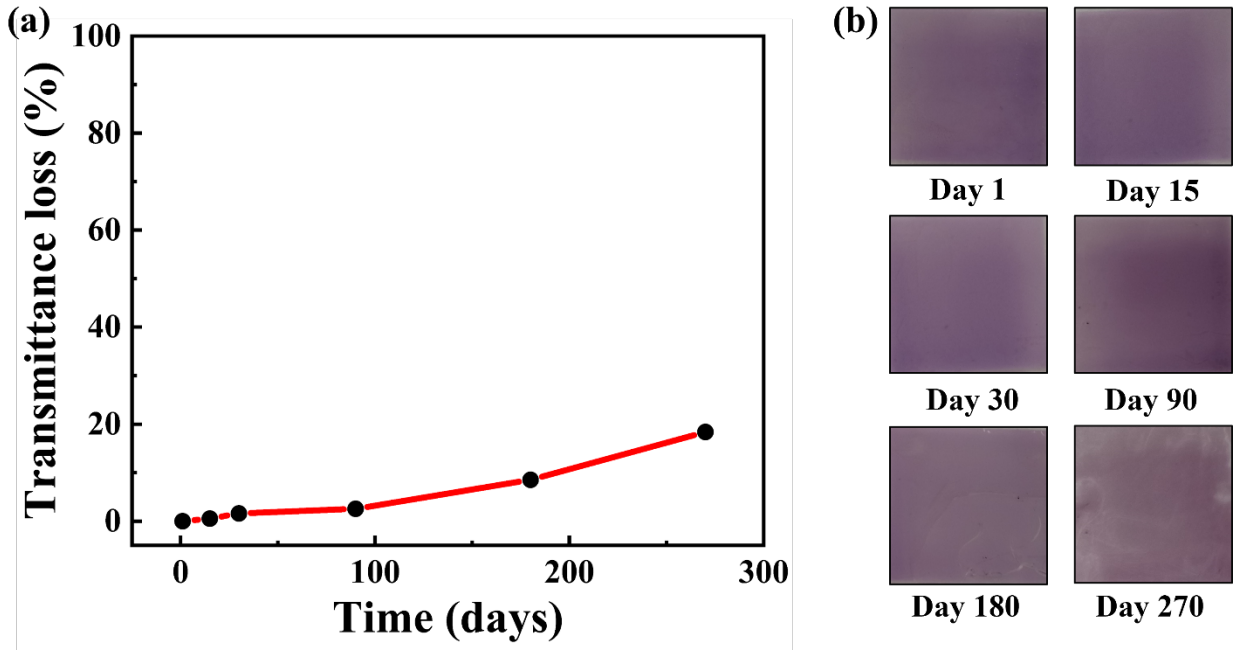

Figure S10. (a) Shelf life of the device stored at 40-50% RH for 9 months, and (b) image of the device over 9 months.

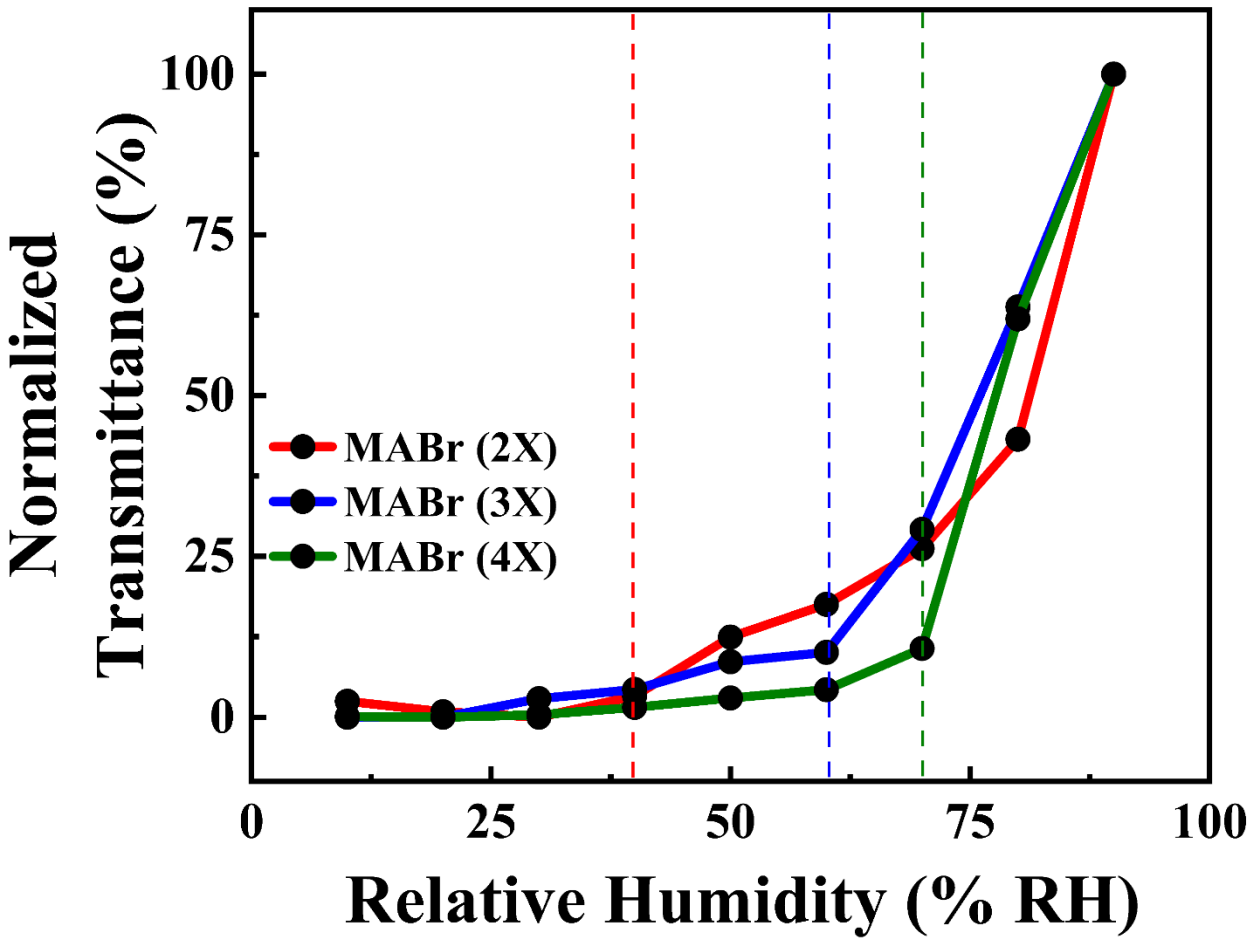

Figure S11. Role of MABr in the active material for the cut-off humidity in the non-linear humidity sensing system.

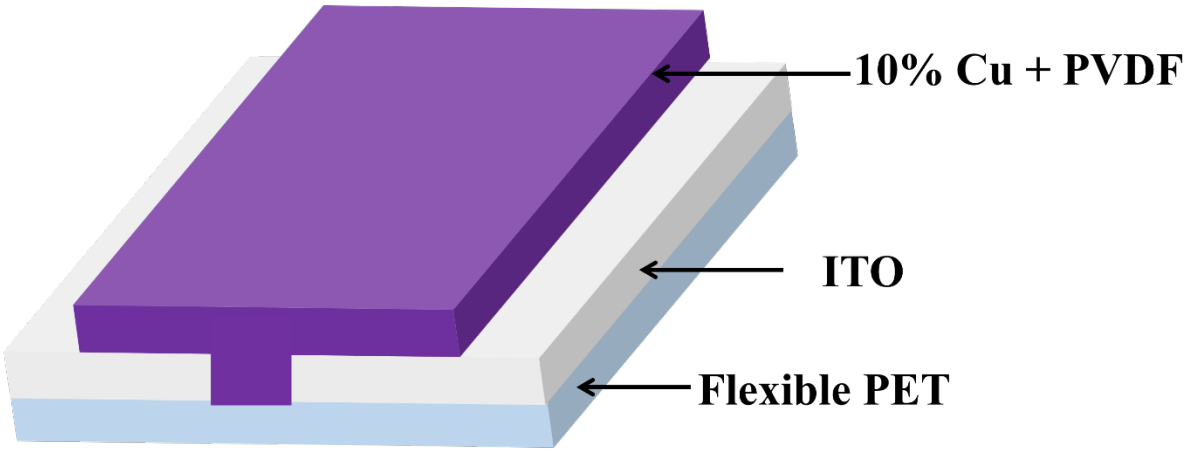

Figure S12. Device schematics for the flexible PTENG device.

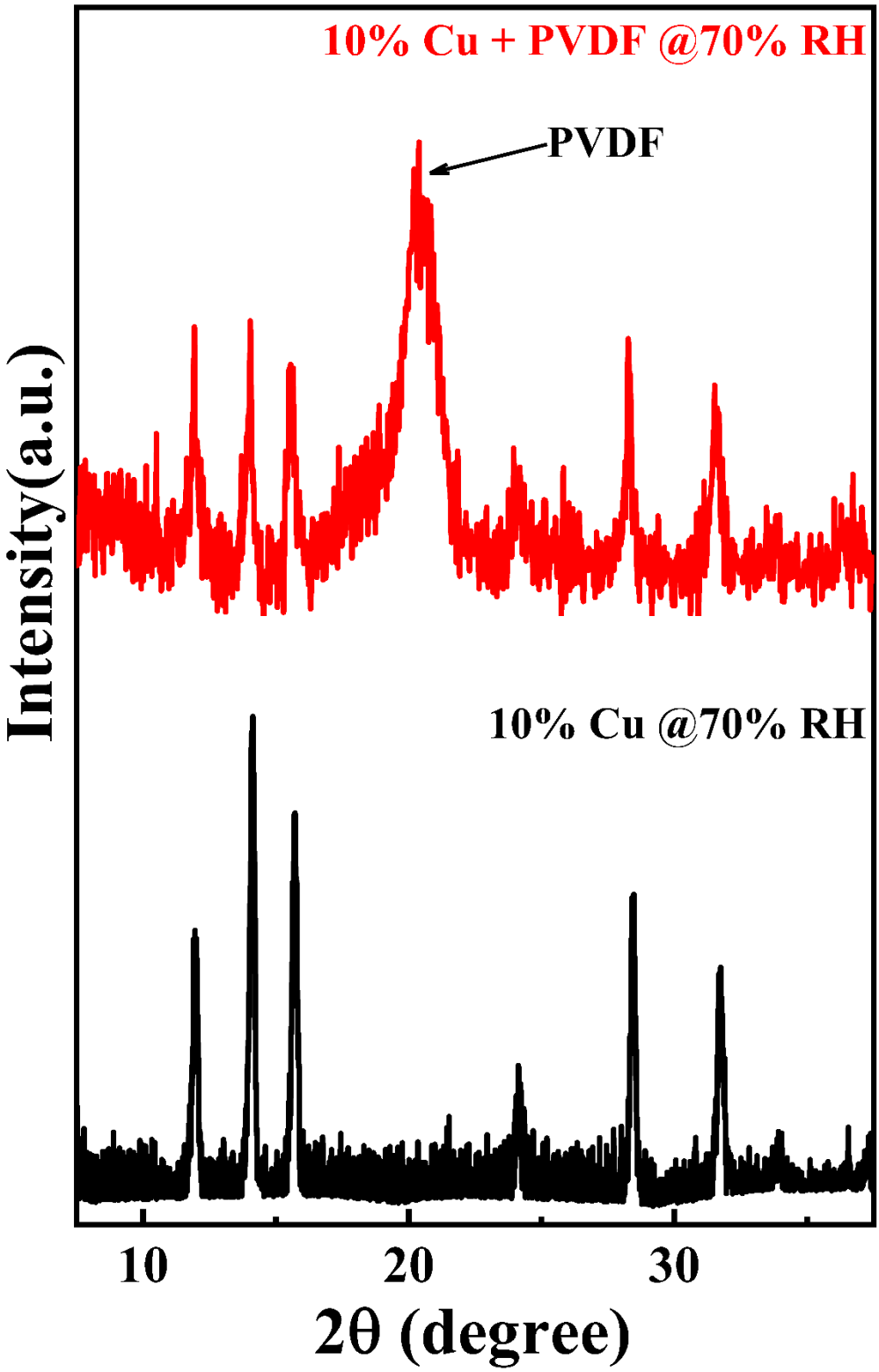

Figure S13. XRD of the 10% Cu + PVDF composite at 70% RH, compared to that of the 10% Cu film at 70% RH.

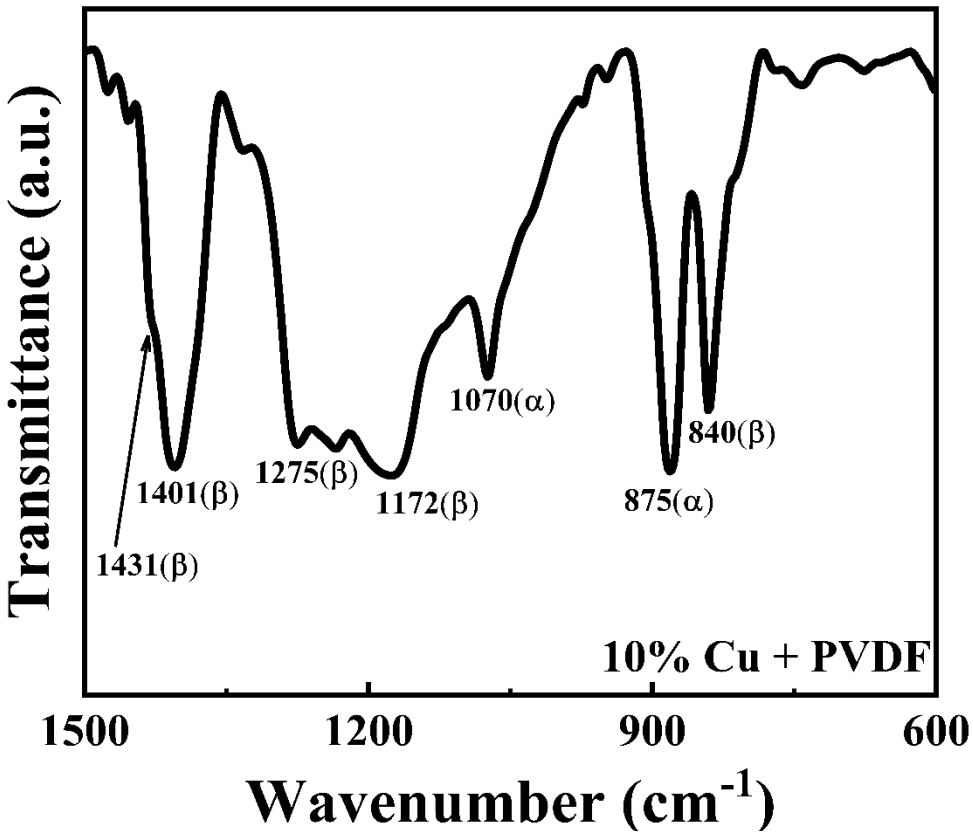

Figure S14. FTIR of the 10% Cu + PVDF composite.

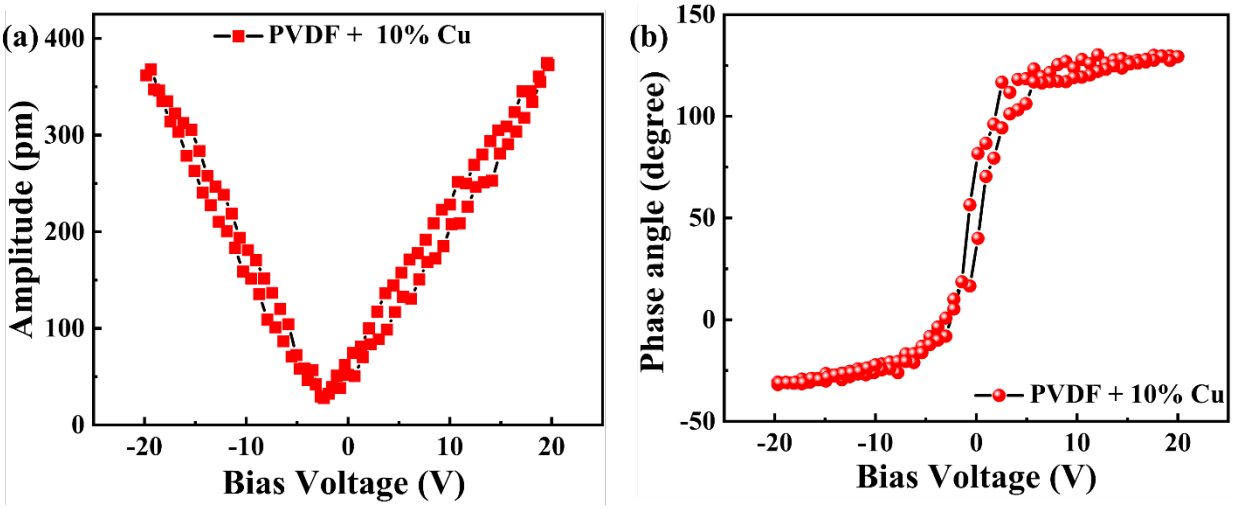

Figure S15. (a) Amplitude- bias voltage loop, and (b) Phase angle-bias voltage loop of the 10% Cu + PVDF composite using Piezo-response Force Microscopy (PFM).

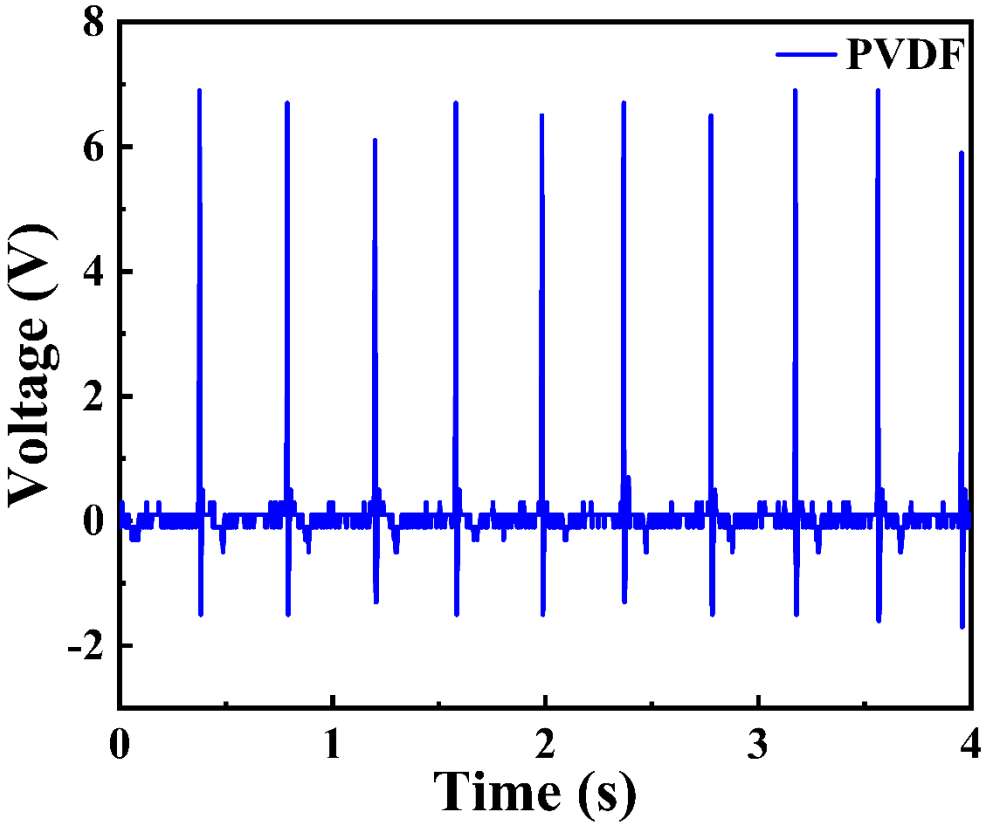

Figure S16. Output generated by flexible PVDF device by hand tapping.

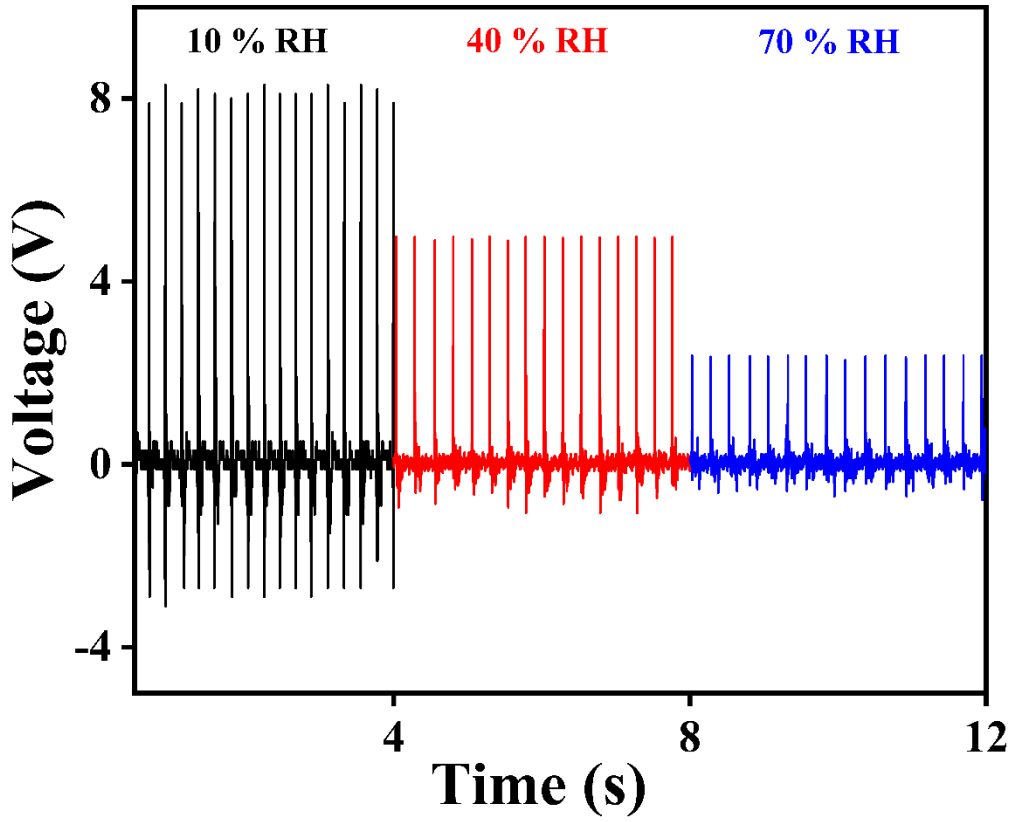

Figure S17. Output generated by flexible 10% Cu + Cellulose acetate device by hand tapping at different % RH.

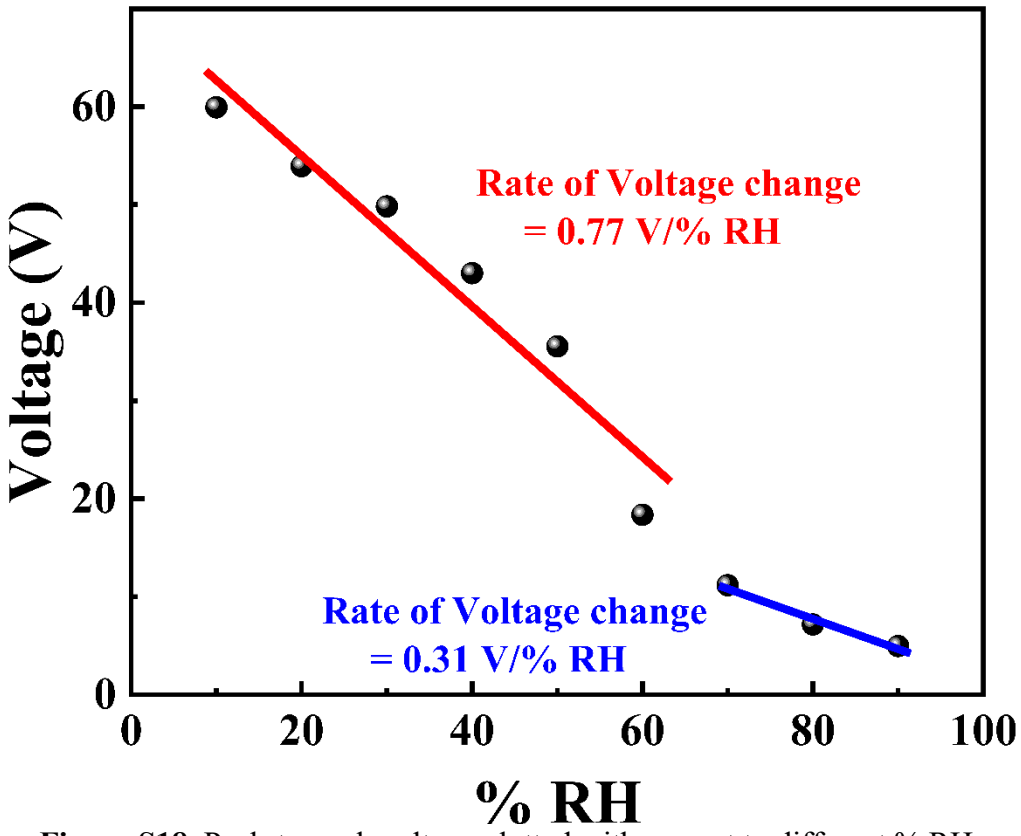

Figure S18. Peak-to-peak voltage plotted with respect to different % RH.

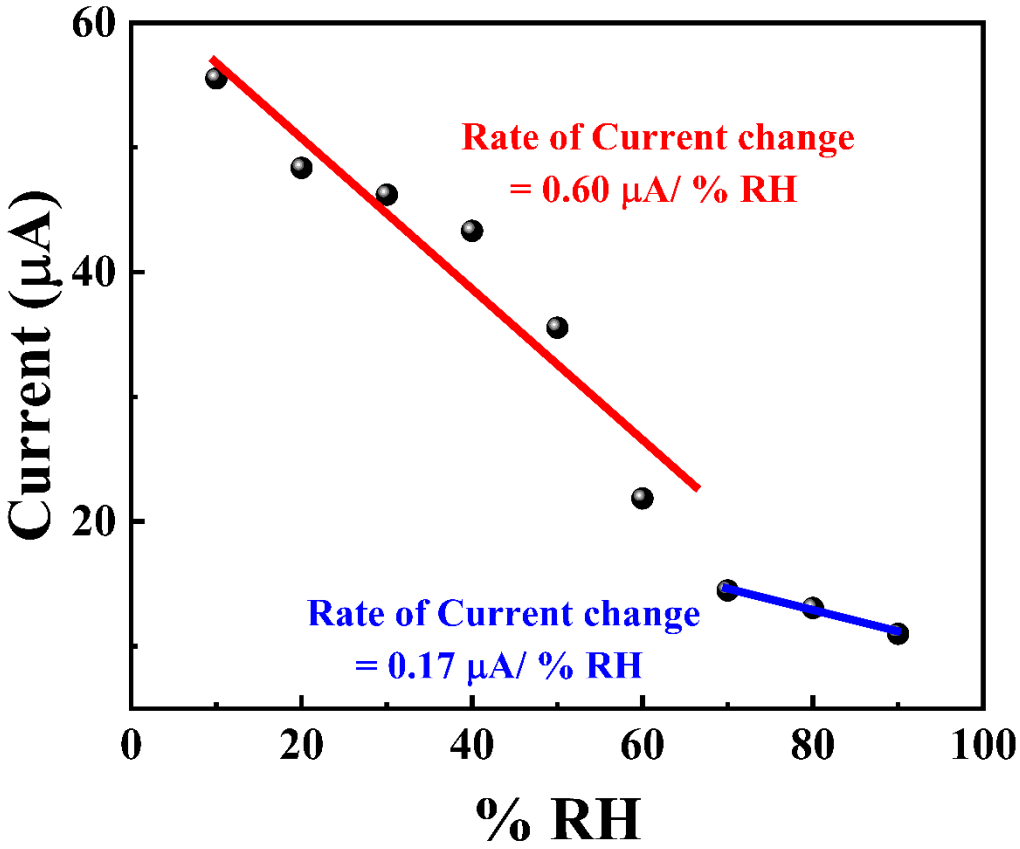

Figure S19. Peak-to-peak current plotted with respect to different % RH.

Table S1. A comparative analysis of optical humidity sensors from published research.

Sl. No.	Material	Material type	Sensor type	Range (%RH)	Response/Recovery (s)	Sensitivity (% RH^{-1})	Behavior	Shelf life (20% drop)	Reference
1.	Cs_4PbBr_6/FAU-Y	Perovskite-zeolite composite	Optical (PL)	7-98	120/300	11.8	Linear	7 days	[1]
2.	$CsPbBr_3$/SAPO-34	Perovskite-zeolite composite	Laser pulse	72-82	-	24%	-	15 h	[2]
3.	MA_2CuBr_4	Perovskite	Absorbance	7-98	200/400	0.00529	Linear	30 days	[3]
4.	$CsPbBr_3$, $CsPbCl_3$, $CsPbCl_{1.5}Br_{1.5}$	Perovskite nanocrystal	Photolumine-scence	30-90	-	-	Non-linear	-	[4]
5.	EMT-$CsPbBr_3$	Zeolite-Perovskite	Photolumine-scence	0-92	3 / -	1978.83 a.u.	Linear	180 days	[5]
6.	$MAPbBr_3$ /TFPP	Perovskite/ Dye	Photolumine-scence	7-98	250/ 30-70	-	Linear	-	[6]
7.	MA_2SnBr_6 caged MA_2CuBr_4	Perovskite	Transmittance	10-90	19/19	0.061 (10-60% RH) 1.31 (70-90% RH)	Non-linear	>270 days	This work

Table S2. Peak-to-peak voltage and current generation of flexible 10% Cu perovskite-PVDF PTENG device on hand hammering at different % RH.

Humidity (%)	Voltage (V)	Current (μA)
10	59.94 (± 2.1)	55.53 (± 1.6)
20	53.94 (± 1.9)	48.36 (± 1.9)
30	49.83 (± 2.1)	46.2 (± 1.5)
40	43.01 (± 1.95)	43.31 (± 1.95)
50	35.56 (± 1.5)	35.55 (± 1.1)
60	18.36 (± 1.05)	21.86 (± 1.3)
70	11.17 (± 0.7)	14.48 (± 1.1)
80	7.18 (± 0.4)	13.08 (± 0.9)
90	4.98 (± 0.3)	11.01 (± 1.1)

Table S3. Peak-to-peak voltage generation of 10% Cu perovskite-PVDF composite over flexible PET based ITO substrate on wrist folding, bending and under heel tapping at different % RH.

Humidity (%)	Wrist folding (V)	Bending (V)	Heel tapping (V)
10	7.42 (± 0.5)	6.16 (± 0.42)	5.02 (± 0.51)
20	7.14 (± 0.4)	4.97 (± 0.33)	4.85 (± 0.37)
30	5.34 (± 0.36)	4.68 (± 0.37)	4.41 (± 0.33)
40	3.78 (± 0.27)	3.89 (± 0.29)	4.31 (± 0.27)
50	2.75 (± 0.19)	3.54 (± 0.28)	3.12 (± 0.13)
60	2.68 (± 0.17)	2.63 (± 0.19)	2.41 (± 0.10)
70	1.74 (± 0.17)	2.53 (± 0.17)	2.04 (± 0.08)
80	1.70 (± 0.19)	1.13 (± 0.09)	1.98 (± 0.12)
90	1.52 (± 0.13)	0.66 (± 0.05)	1.57 (± 0.07)

Table S4. Peak-to-peak voltage generation of 10% Cu perovskite-PVDF composite over flexible PET based ITO substrate on finger tapping under saturated vapours of interfering gases at 10% RH.

Interfering gas species	Peak to peak voltage
10% RH	59.94 (± 2.1)
Ethanol	17.7 (± 0.12)
Hexane	7.633 (± 0.34)
Toluene	9.96 (± 0.26)
DCM	2.99 (± 0.12)
Acetone	7.031 (± 1.09)
Ethyl Acetate	7.056 (± 0.61)
Diethyl ether	3.67

Table S5. Comparison of humidity sensing parameters of PTENG devices from the literature.

Sensor materials	Humidity range	Voltage	Response/recovery time	Reference
Ga/ZnO	45–80% RH	0.6 V (~45% RH)	5 s (90%)	[7]
Al-ZnO_2	15-60% RH	0.8 V (~15% RH)	4/7 s	[8]
Cd-ZnO Nanowires	30-70% RH	0.6 V (~30% RH)	-	[9]
TiO_2	20-90% RH	100-200 mV	4.5/2.8 s	[10]
$NaNbO_3$	5-95% RH	2 V	12 s	[11]
Sm-PMN-PT ceramic	0-100% RH	1.5 V (~20% RH)	~20 s	[12]
PVDF+10% Cu	10-90% RH	60 V (~10% RH)	-	This work

References:

1 Y. J. Gao, G. Romolini, H. Huang, H. Jin, R. A. Saha, B. Ghosh, M. De Ras, C. Wang, J. A. Steele, E. Debroye, J. Hofkens and M. B. J. Roeffaers, *J Mater Chem C Mater*, 2022, 10, 12191–12196.

2 R. Li, J. Yu, S. Wang, Y. Shi, Z. Wang, K. Wang, Z. Ni, X. Yang, Z. Wei and R. Chen, *Nanoscale*, 2020, 12, 13360–13367.

3 H. Lee, D. Lee, H. Jin, D. Baek, M. K. Kim, J. Cha, S. K. Kim and M. Kim, *Nanoscale Adv*, 2022, 4, 3309–3317.

4 feng xuliang, liu yuanxun, huang zhihao, gu shuichong, Z. X. Xuan-yu, S. zi-jun zijun, L. Cheng-hua, C. Huajin and li ruxue, *https://doi.org/10.1117/12.2661984*, 2023, 12565, 278–285.

5 X. Zhang, J. Lv, J. Liu, S. Xu, J. Sun, L. Wang, L. Xu, S. Mintova, H. Song and B. Dong, *J Colloid Interface Sci*, 2022, 616, 921–928.

6 W. Xu, F. Li, Z. Cai, Y. Wang, F. Luo and X. Chen, *J Mater Chem C Mater*, 2016, 4, 9651–9655.

7 T. Zhao, Y. Fu, Y. Zhao, L. Xing and X. Xue, *J Alloys Compd*, 2015, 648, 571–576.

8 W. Zang, W. Wang, D. Zhu, L. Xing and X. Xue, *RSC Adv*, 2014, 4, 56211–56215.

9 B. Yu, Y. Fu, P. Wang, Y. Zhao, L. Xing and X. Xue, *Physical Chemistry Chemical Physics*, 2015, 17, 10856–10860.

10 D. Shen, M. Xiao, Y. Xiao, G. Zou, L. Hu, B. Zhao, L. Liu, W. W. Duley and Y. N. Zhou, *ACS Appl Mater Interfaces*, 2019, 11, 14249–14255.

11 L. Gu, D. Zhou and J. Cheng Cao, , DOI:10.3390/s16060833.

12 S. Y. Su, Z. Yuan, J. Zou, G. Xie, J. Chen, Y. Su, Y. Liu, W. Li, X. Xiao, C. Chen, H. Lu, H. Tai and Y. Jiang, *Cite this: Mater. Horiz*, 2023, 10, 842.